Journal of Magnetic Resonance 301 (2019) 80–84

Contents lists available at ScienceDirect

Journal of Magnetic Resonance

journal homepage: www.elsevier.com/locate/jmr

# Quick, selective NMR spectra of C—OH moieties in $^{13}$C-enriched solids

Pu Duan, Klaus Schmidt-Rohr *

*Department of Chemistry, Brandeis University, Waltham, MA 02453, United States*

ARTICLE INFO

*Article history:*
Received 31 July 2018
Revised 21 February 2019
Accepted 26 February 2019
Available online 27 February 2019

*Keywords:*
Spectral editing
Hydroxyl-proton selection (HOPS)
Orthodiphenols
Aromatic ethers
NMR of carbon materials
NMR of hydrochar

ABSTRACT

A convenient one-dimensional magic-angle spinning NMR method is presented that provides selective NMR spectra of COH moieties in uniformly $^{13}$C-enriched organic materials. This method, termed hydroxyl-proton selection (HOPS), eliminates the magnetization of protons directly bonded to carbons by recoupling the $^{1}$H–$^{13}$C dipolar interaction for a short time (~70 μs), which also serves as a chemical-shift filter to suppress $^{1}$H magnetization of $CH_3$ groups. After cross polarization to $^{13}$C, the signals of C—OH and COOH carbons are observed selectively. This makes it possible to distinguish alcohols from ethers, in particular phenols from aromatic ethers such as the furans often formed by dehydration of glucose, and carboxylic acids from carboxylates and ethers. HOPS NMR reveals that orthodiphenols are often a major component of low-temperature carbon materials. For instance, it forces the reassignment of the 143 ppm $^{13}$C NMR signal of hydrothermal carbon to such catecholic diphenols, while a previous NMR-based structural model had attributed this peak to a central furan–furan linkage.



## 1. Introduction

Detailed structure determination in uniformly $^{13}$C-enriched organic solids by magic-angle-spinning nuclear magnetic resonance (MAS NMR) has come to be widely used in structural biology, biophysics, and materials science [1–7]. Proteins are routinely biosynthesized from $^{13}$C-enriched glucose [1–7], which is a relatively inexpensive starting material. In addition, many different forms of uniformly $^{13}$C-enriched biomass are now available [8]. Furthermore, a wide variety of chars have been produced by pyrolysis or browning reactions, and their structural features can be studied in model materials made from $^{13}$C-enriched glucose [5–7], since pyrolysis temperature is the dominant factor controlling char composition. Pyrolyzed carbohydrates are promising materials for hydrothermally stable catalyst supports [9], pollution remediation [10,11], carbon sequestration e.g. in biochar, anodes for lithium ion batteries [12,13], supercapacitors [14–16], and gas separation or storage [17], but their structures are complex and still contentious [5,18–20]. Graphite oxide, a potential precursor of graphene, can be uniformly $^{13}$C enriched using $^{13}CH_4$ [3]. In all these materials, the $^{13}$C chemical shifts of the resonances observed reflect substitution of carbons by heteroatoms, while detailed information on bonding in the carbon backbone is obtained from two-dimensional $^{13}$C–$^{13}$C NMR spectra [3,5,21,22], possibly enhanced by spectral editing [23–25].

What is more difficult to assess by traditional NMR is the protonation state of oxygen substituents. Since OH groups are often crucial for the interactions of materials or molecules with their surroundings, this is a significant limitation of current NMR technology. Alcohols (C—OH) and ethers (C—O—C) have overlapping $^{13}$C chemical shift ranges; in particular, C—O carbons in phenols and in furans, i.e. cyclic aromatic ethers, both resonate between 140 and 160 ppm, and both structures can be formed by sugar pyrolysis [5–7]. Carboxylic acids (COOH) and carboxylates ($COO^-$), which participate in intermolecular interactions through hydrogen bonding and salt bridges, respectively, as well as esters (COOC) produce overlapping resonances between 163 and 185 ppm. COOH groups can sometimes be assigned based on their $^{1}$H resonances at >9 ppm in two-dimensional $^{1}$H-$^{13}$C NMR spectra, but it would be desirable to identify them without requiring an additional spectral dimension.

Here we present a simple, robust, and efficient method, termed hydroxyl-proton selection (HOPS), that suppresses the $^{1}$H magnetization of $^{13}$C-$^{1}$H moieties but retains OH (and NH) magnetization that can be observed in $^{1}$H NMR or used as the sole magnetization source in cross polarization (CP) to $^{13}$C, providing selective $^{13}$C NMR spectra of C—OH moieties. We demonstrate that this method can identify diphenol signals previously misassigned to furanoic backbone sites, upending a central structural feature of a previous NMR-based model of hydrothermal carbon.

* Corresponding author.
*E-mail address:* srohr@brandeis.edu (K. Schmidt-Rohr).

https://doi.org/10.1016/j.jmr.2019.02.007
1090-7807/

## 2. Materials and methods

### 2.1. Materials.

Uniformly $^{13}$C-enriched glucose, uniformly $^{13}$C/$^{15}$N-enriched tyrosine, and deuterium oxide were purchased from Cambridge Isotopes.

All the $^{13}$C-enriched carbon materials were made from uniformly $^{13}$C-enriched glucose. The glucose treated with fuming sulfuric acid, referred to as "Direct" sulfonated carbon [6], and the hydrothermal glucose char were synthesized as reported in our previous publication [6]. Briefly, for direct sulfonation glucose was placed in fuming $H_2SO_4$ and heated to 150 °C for 2 h. The solid was washed with water and dried overnight at 100 °C. Hydrothermal glucose char was produced from dissolved glucose held at 500 psi and 200 °C for 18.5 h. The solid was filtered, washed with water, and dried overnight at 100 °C. Regular chars were made by glucose pyrolysis at 400 °C and at 500 °C in a horizontal tube furnace under flowing (~1 L/min) $N_2$ gas. After an initial treatment for 1 h, the material was cooled, ground into a powder with mortar and pestle, and pyrolyzed for an additional 9 h. The solution-caramelized glucose was produced by heating a sealed glucose solution buffered at pH = 8.5 at 100 °C for a week, followed by filtering, dialysis, and freeze-drying.

The U-$^{13}$C, $^{15}$N-L-tyrosine was packed into a 4-mm rotor as received. The 87% labile-proton-deuterated U-$^{13}$C-tyrosine (87% H/D exchanged U-$^{13}$C-tyrosine) was prepared by exchange in deuterium oxide with the following procedure. 10 mg of sample was first dissolved in 5 μL de-gassed deuterium oxide at 90 °C in a 100 mL round bottom flask. Then, the solution was stirred under $N_2$ protection for 1 h. The flask was sealed and kept in the dark at room temperature. The suspension that formed overnight was centrifuged at 14,000 rotations per minute and 0 °C for 10 min, and the supernatant was removed. This procedure was repeated three times. Finally the sample was lyophilized and center-packed into a 4-mm rotor.

### 2.2. NMR parameters

The NMR experiments were performed on a Bruker Avance 400 spectrometer at 400 MHz $^1$H and 100 MHz $^{13}$C resonance frequencies, using a 4-mm double-resonance probehead. All the spectra were measured at a spinning frequency of $\nu_r$ = 14 kHz. $^{13}$C and $^1$H 90° pulse lengths were 4.2-μs steps. The $^1$H direct polarization spectra were collected with background suppression by doubling of the excitation-pulse length [26]. The $^1$H HOPS spectra were collected without probe-head background suppression, because the background signal from the first 90° pulse is dephased during the 70-μs period, and that from the second 90° pulse will be phase-cycled away. The ramped cross polarization used in HOPS was implemented with a 11-step linear amplitude ramp on $^1$H from 90% to 100% pulse strength, with 25-μs steps. The recycle delay was 1 s for all the HOPS $^{13}$C spectra of carbon materials, and 512 scans were averaged. The reference full spectrum of U-$^{13}$C–tyrosine, dashed curve in Fig. 2a, was collected after composite-pulse multiCP [27] with a 3-s recycle delay and seven 1-s $^1$H repolarization and $^{13}$C spin equilibration periods. All the other reference full spectra, shown by dashed curves in Figs. 3-5, were collected after one-pulse excitation (direct polarization, DP), with 30–200-s recycle delays for nearly complete relaxation to thermal equilibrium. The $^1$H decoupling field strength during detection was $\gamma B_1/(2\pi)$ = 60 kHz.

## 3. Results and discussion

### 3.1. Principle of HOPS

The central feature of HOPS is suppression of C—H proton magnetization by $^1$H{$^{13}$C} rotational echo double resonance (REDOR)

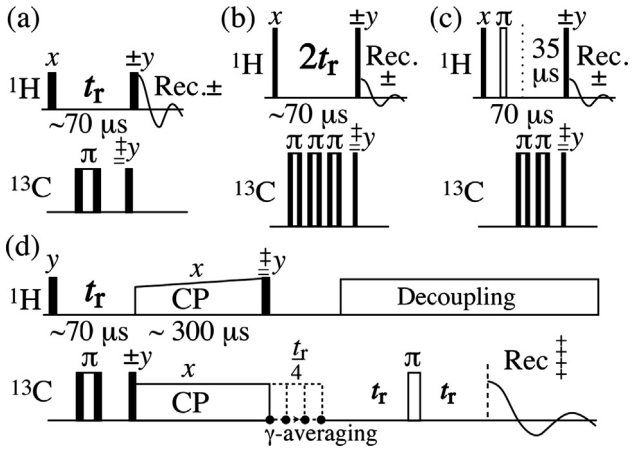


**Fig. 1.** Pulse sequences (filled rectangles: π/2-pulses; narrowest open rectangles: π-pulses) for hydroxyl proton selection (HOPS) with (a-c) direct $^1$H NMR detection at (a) ~14 kHz MAS and (b) ~28 kHz MAS in a 9.4 T field. (c) Pulse sequence for ~28 kHz MAS in a 18.8 T field, with a 35-μs chemical shift filter. For the $S_0$ spectrum (without the composite $^{13}$C π-pulses), the $^1$H π-pulse should be shifted to the center of the $^1$H evolution period. (d) $^{13}$C NMR detection after rampCP, "γ-averaging" [31] for sideband artifact suppression (see the SI) and a Hahn spin echo. The phase-cycled ±$y$ π/2-pulses are discussed in the SI. The reference spectrum $S_0$ is obtained by omitting the composite $^{13}$C π-pulses. The pulse sequence code can be found in the SI and at http://www.ksrlab.org/nmrksr/.

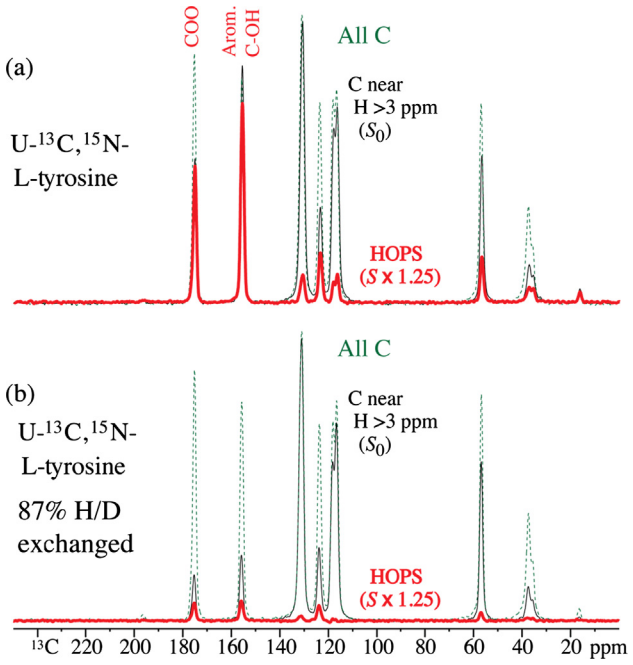


**Fig. 2.** (a) HOPS $^{13}$C NMR spectrum $S$ (thick line) of uniformly $^{13}$C/$^{15}$N-enriched tyrosine and reference spectrum $S_0$ (thin line) with ramped cross polarization of 0.28 μs, at 14 kHz MAS. The HOPS spectrum has been scaled up by 1.25. For reference, a corresponding full multiCP spectrum (dashed lines) is also shown, scaled to approximately match the $S_0$ CH signals between 115 and 130 ppm. (b) Corresponding spectra after 87% H/D exchange. Reduced intensities of the COO and COH peaks after short cross polarization and in the HOPS spectrum confirm that all the HOPS signals in (a) are due to cross polarization from OH and $NH_3^+$.

[28], taking advantage of the strong ($\delta_{C\text{-}H} \geq 20$ kHz) one-bond dipolar coupling of C—H protons to $^{13}$C in uniformly $^{13}$C-enriched solids. The one-bond $^1$H{$^{13}$C} interaction is recoupled by composite π-pulses ($90°_x$ $180°_y$ $90°_x$) on $^{13}$C, one or three depending on the spinning frequency, see Fig. 1a and b, and it dephases the C—H proton magnetization within 70–90 μs: The spin-pair REDOR curve decays to 0 ± 5% for a decoupling time between $t_r = 1.45/\delta_{C\text{-}H}$ and $2.3/\delta_{C\text{-}H}$ [23,28], corresponding to 68 and 110 μs for

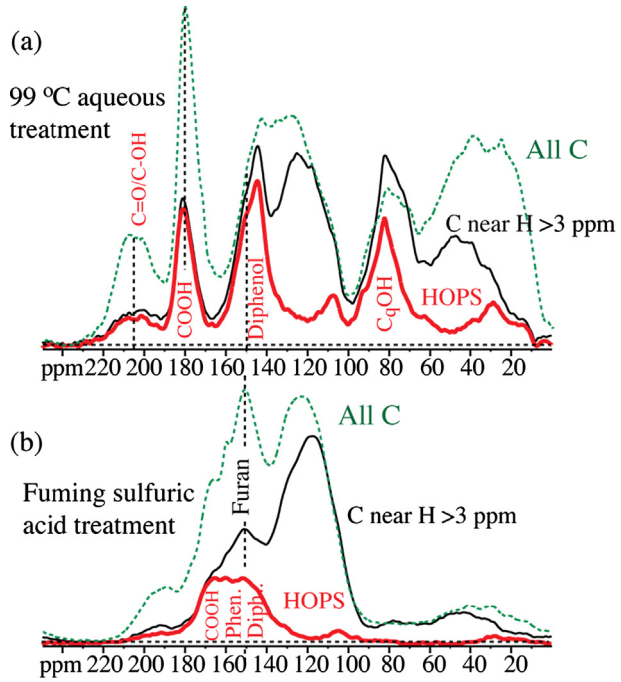


**Fig. 3.** HOPS $^{13}C$ NMR spectra $S$ (thick lines) with reference spectra $S_0$ (thin lines) and corresponding full direct-polarization spectra (dashed lines) of uniformly $^{13}C$-enriched (a) high-molecular weight fraction of solution-caramelized glucose, revealing orthodiphenol signals at 144 ppm (see also Fig. S2), and (b) glucose treated with fuming sulfuric acid, showing COOH (rather than esters) at 164 ppm. Each HOPS spectrum has been scaled up by 1.25, while each full spectrum (dashed) was scaled to match the $S_0$ signal near 110 ppm. Spinning frequency: 14 kHz; cross-polarization time: 0.28 ms.

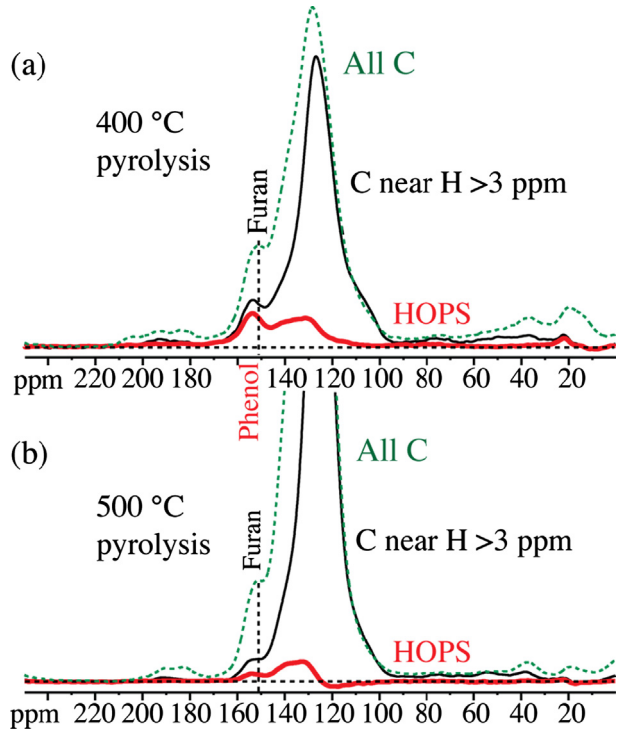


**Fig. 4.** HOPS, reference $S_0$, and corresponding full direct-polarization spectra of chars made by pyrolysis at uniformly $^{13}C$-enriched glucose at (a) 400 °C and (b) 500 °C. The line types, scaling, and experimental parameters were the same as in Fig. 3.

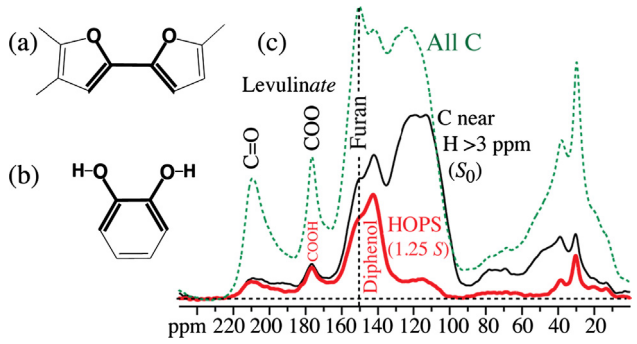


**Fig. 5.** Backbone analysis of hydrothermal carbon based on HOPS NMR. (a) An important piece of the structural model of Ref. [5], with the central 142-ppm aromatic C—O—$^{13}$C—$^{13}$C—O—C spin pair highlighted. (b) Corresponding similar H—O—$^{13}$C—$^{13}$C—O—H spin pair, with nearly indistinguishable $^{13}C$ chemical shifts, in a catecholic diphenol. (c) HOPS $^{13}C$ NMR spectrum $S$ (thick line) of uniformly $^{13}C$-enriched hydrothermal carbon scaled by 1.25, reference spectrum $S_0$ (thin line) with $^{1}H$ chemical-shift filter, and corresponding direct-polarization spectrum of all carbons (dashed line), scaled to match near 110 ppm.

$\delta_{C\text{-}H}$ = 21 kHz. The reference spectrum $S_0$ is obtained by leaving out the composite π-pulses on the $^{13}C$ channel.

Similar recoupled $^{1}H\{^{13}C\}$ dephasing is also a feature of the 2D medium-and-long-distance (MELODI) HetCor experiment [29], but HOPS is much simpler to implement, replacing a difficult, rarely used niche method with a convenient routine experiment. While MELODI HetCor involves pulsed $^{1}H$ homonuclear decoupling, heteronuclear recoupling as well as 2D data acquisition and has rarely been applied to carbon materials, HOPS is a simple one-dimensional experiment.

HOPS relies not on pulsed decoupling but on moderately fast MAS to refocus the $^{1}H$ homonuclear dipolar evolution of the OH protons at the end of one or two rotation periods, which makes the experiment straightforward and robust. Since OH protons are subject to no geminal (2-bond) and only one if any vicinal (3-bond) dipolar coupling when the C—OH carbon is $sp^2$-hybridized, their dipolar $T_2$ relaxation loss during the ~70-μs selection period is relatively minor compared with that of most immobile $CH_2$ and CH groups, which helps with the OH magnetization selection.

During the 70- to 90-μs $^{1}H$ dipolar dephasing period, $^{1}H$ chemical shift evolution occurs and produces a phase or amplitude modulation of the detected signal. Rather than refocusing this evolution into a spin echo, which would require an additional pulse, we utilize the unrefocused evolution time $t_{HOPS} \approx 70$ μs, or a fraction of it, for chemical-shift filtering, i. e. modulation of the observed intensity by $\cos(\omega t_{HOPS})$, where ω is the $^{1}H$ chemical shift (more precisely, the resonance offset) of the peak in question [30]. The goal of the chemical-shift filter is suppression of the proton magnetization of $CH_3$ groups. These otherwise produce undesirable background signals, since the methyl rotational jumps motionally average the C—H dipolar coupling by a factor of three and therefore prevent full C—H dipolar dephasing of methyl protons during $t_{HOPS} \approx 70$ μs. With the timings shown in Fig. 1a, peaks 3.6 kHz off resonance are suppressed. Thus magnetization of $CH_3$ (and mobile-$CH_2$) protons resonating near 1.5 ppm is suppressed or inverted if the irradiation frequency is chosen near 10.5 ppm at 400 Hz/ppm, and near 9 ppm at 600 Hz/ppm. At 800 Hz/ppm, a spinning speed of 28 kHz should be used and the pulse sequence of Fig. 1c, where the first π-pulse has been moved to the $^{1}H$ channel; this results in 35 μs of chemical shift filtering during the second half of the 70-μs dipolar recoupling period. The chemical-shift filtering using the sequences of Fig. 1a and 1b also occurs without the $^{13}C$ recoupling pulse(s), so the reference $S_0$ spectrum can,

somewhat simplistically, be described as arising from $^{1}H$ resonating at >3 ppm.

Note that exchange of the OH protons with $H_2O$ does not interfere with the hydroxyl proton selection, but actually makes it more efficient since it further weakens the OH-to-C dipolar coupling. HOPS is quite efficient since the simple $^{1}H\{^{13}C\}$ dipolar, chemical-shift, and $T_{2H}$ selections of OH proton magnetization occur concurrently within a relatively short time of ~70 μs.

For $^{13}C$-enriched materials without OH or NH groups and little adsorbed $H_2O$, such as char made by pyrolysis of $^{13}C$-glucose at 500 °C, the overall $^{1}H$ signal after HOPS is strongly suppressed as intended, see Fig. S1a, to an integrated value close to zero. When OH groups are significantly present, see Fig. S1c and S1e–g, a signal with only small dipolar spinning sidebands remains, characteristic of OH protons with their relatively weak homo- and heteronuclear dipolar couplings. At the spinning frequency of 14 kHz, the spectral resolution just from MAS alone is not sufficient to identify specific OH groups, but the amount of OH (including $H_2O$) in the sample could be estimated.

### 3.2. HOPS with $^{13}C$ detection

By relatively short cross polarization from the HOPS-selected OH protons to nearby $^{13}C$ spins, see Fig. 1d, a selective $^{13}C$ spectrum of the COH groups can be obtained. During CP, the relevant component of the $^{1}H$ magnetization vector is projected onto the spin-lock field, producing the $\cos(\omega t_{HOPS})$ modulation that suppresses $CH_3$ magnetization.

Fig. 2a displays the HOPS $^{13}C$ spectrum (thick red line; *S* in the standard REDOR nomenclature) of $^{13}C$-enriched tyrosine and the corresponding reference spectrum $S_0$ without $^{13}C\{^{1}H\}$ dephasing (but still with $^{1}H$ chemical-shift filtering). While its neighboring aromatic C—H show only weak signals, the aromatic C—OH peak is prominently retained (>75%) in the HOPS spectrum. Here and in the other HOPS spectra shown below, we find it advantageous to scale up the HOPS spectra by 1.25 to compensate for partial signal loss by $^{1}H$—O—$^{13}C$ two-bond dephasing. The intensity of the C—OH peak in the HOPS spectrum is 23% of that in the corresponding full rampCP spectrum (35% relative to 0.28-ms rampCP). This demonstrates that HOPS provides adequate signal in typical rigid organic solids. The COO group is apparently polarized by the $NH_3$ protons to which it is hydrogen bonded. In uniformly $^{13}C/^{15}N$-enriched proteins, the signal of C bonded to N-H could be suppressed by optimized $^{13}C\{^{15}N\}$ REDOR [23]. The HOPS spectrum of tyrosine-$d_4$ exchange-deuterated from $D_2O$, where most of the OH and $NH_3$ protons have been replaced by deuterons, is shown in Fig. 2b. It exhibits little signal, confirming that the signals observed in the HOPS spectrum of Fig. 2a originate from OH and $NH_n$ proton magnetization.

### 3.3. HOPS of carbon materials

$^{13}C$ HOPS spectra of several $^{13}C$-enriched carbon materials and corresponding reference spectra $S_0$ without $^{13}C\{^{1}H\}$ dephasing, as well as quantitative direct-polarization spectra, are presented in Figs. 3–5. In these aromatic-rich materials made under hydrothermal or pyrolysis conditions from $^{13}C$-glucose, HOPS is again seen to be highly selective, retaining prominent signals only of OH-bonded carbons. Signals of carboxylic acids between 180 and 164 ppm, phenols near 152 ppm, diphenols near 143 ppm, acetals or ketals (O—C—OH) around 105 ppm, and primary (62 ppm), secondary (75 ppm) or tertiary (80–92 ppm) alcohols are selectively preserved.

In solution-caramelized glucose, the HOPS spectrum shows a strong COH peak at 143 ppm (Fig. 3a). This chemical shift is characteristic of 1,2-dihydroxy-substituted aromatic rings; indeed, a dominant diagonal peak in $^{13}C$—$^{13}C$ correlation NMR confirms that most of the 143-ppm carbons are bonded to each other (see Fig. S2). Thus, HOPS has elucidated the previously uninterpretable aromatic bands of this material in terms of catecholic diphenols, which had not been prominently proposed before. A shoulder near 152 ppm assigned to other phenols, a COOH peak near 180 ppm, and C—OH signal near 82 ppm (mostly $C_qOH$, nonprotonated "quaternary" carbon) are also observed in the HOPS spectrum with strong intensities. Interestingly, some ketone signals near 205 ppm are retained in the HOPS spectrum, which may be due to keto-enol ($H_nC$—C=O ↔ $H_{n-1}C$=C—OH) tautomerism or hydrogen bonding; this question will be further investigated in the future.

Glucose chemically oxidized by fuming sulfuric acid also shows COOH, phenol, and orthodiphenol bands after HOPS, see Fig. 3b, but the pronounced peak at 152 ppm in the full spectrum does not contribute much to the HOPS spectrum and must therefore be assigned to aromatic ethers like furans; this is consistent with our previous analysis [6]. Fig. 4a shows that in a char made by pyrolysis at 400 °C, HOPS resolves a phenolic peak with a chemical shift of 154 ppm, but this is only a small fraction of the aromatic C—O signal. In the spectrum of all carbons, aromatic ethers, presumably furanoic, are dominant. Their peak maximum at 152 ppm is distinct from that of the phenols in HOPS, see Fig. 4a, confirming that these are two different chemical species. The phenol fraction is seen to decrease further, relative to aromatic ethers, in a corresponding 500 °C char (Fig. 4b).

### 3.4. Orthodiphenols in hydrochar

Fig. 5 demonstrates that even in a well-studied material, HOPS can reveal unexpected structural features that had not been identified based on vibrational spectroscopy or advanced 2D $^{13}C$—$^{13}C$ NMR [5]. The figure shows spectra of hydrothermal carbon or hydrochar made from $^{13}C$-enriched glucose in pressurized water at 180–200 °C, a material which has attracted significant interest in recent years [5,18–20]. The peak at 142 ppm, which produces a distinctive diagonal peak in $^{13}C$—$^{13}C$ correlation spectra [5], has been assigned to pairs of α-carbons of two linked furan rings (C—O—C—C—O—C) [5] without OH groups, see Fig. 5a. The HOPS spectrum with a pronounced peak of C—OH groups at 142 ppm shows that this assignment is incorrect and thus overturns a central feature of the structural model of ref. [5]. Instead, the 142-ppm peak must be assigned to diphenols as sketched in Fig. 5b. Further evidence for such a catecholic structure, which has not been considered in most models of hydrothermal carbon [5,18–20], will be presented elsewhere. The low intensity of the COOH signal in the HOPS spectrum indicates that it is not levulinic acid [5] but levulinate that gives rise to sharp peaks at 177, 210, 38, and 30 ppm in the spectrum of all carbons.

### 3.5. Comparison with other NMR techniques

HOPS shares the $^{1}H\{^{13}C\}$ dipolar dephasing principle with MELODI HetCor NMR [29], but it is much simpler to implement and an order of magnitude faster to complete, since MELODI HetCor requires acquisition of a dipolar-modulated two-dimensional spectrum under pulsed homonuclear $^{1}H$ decoupling. Both methods could not select the signals of C—OH groups in samples without $^{13}C$-enrichment, since the magnetization of $^{1}H$ bonded to $^{12}C$ would remain undephased like that of the C—OH protons.

A reviewer proposed in passing that C—OH and C—O-C moieties might alternatively be distinguished by $^{1}H$-detected fast MAS NMR, but it is not obvious that orthodiphenols could be differentiated from monophenols as easily with $^{1}H$ detection as in a HOPS

spectrum, where the characteristic $^{13}C$ chemical shift of ~143 ppm immediately identifies orthodiphenols. Furthermore, C—O—C and C=O moieties not bonded to OH would be essentially silent in $^{1}H$-detected spectra, while they can be detected and analyzed in HOPS $S_0$ or corresponding quantitative $^{13}C$ NMR spectra, as demonstrated in Figs. 3b, 4, and 5. Implicit in the requirement of $^{13}C$-enrichment for HOPS is very strong $^{13}C$ signal of the samples studied and therefore little need for signal enhancement by $^{1}H$ detection. The HOPS spectra presented here were recorded within 10–30 min and have excellent signal-to-noise ratios.

## 4. Conclusions

We have presented a convenient 1D NMR method for hydroxyl-proton selection in $^{13}C$-enriched materials that not only resolves monophenol from furan signals, but has also revealed catecholic orthodiphenols resonating near 143 ppm, which have rarely been considered in structural models of carbon materials. HOPS also shows signals of protonated COO groups, including aromatic-bonded COOH resonating at ~165 ppm that would traditionally be assigned to esters. Since the $^{13}C$ NMR signal of $^{13}C$-enriched materials is usually quite strong and because $^{1}H\{^{13}C\}$ recoupling, $^{1}H$ chemical-shift filtering, and $T_{2H}$ selection occur concurrently within only 70 μs, little signal averaging is required to obtain a HOPS spectrum. For instance, the HOPS spectra in Fig. 3 were obtained within 10 min of measuring time. HOPS is so simple to run, under the same conditions as quantitative $^{13}C$ NMR, that we apply it routinely to the uniformly $^{13}C$-enriched chars, protective carbon overlayers on mesoporous catalyst supports, Maillard-reaction products, and biomass samples studied in our laboratory.

## Acknowledgements

The authors thank Xiaowen Fang, Jason M. Anderson, and Robert L. Johnson for the preparation of the solution-caramelized glucose, hydrothermal carbon, and pyrolyzed $^{13}C$-glucose, respectively. This research was supported by the Center for Biorenewable Chemicals (CBiRC) funded by NSF grant EEC-0813570.

## Appendix A. Supplementary material

Supplementary data to this article can be found online at https://doi.org/10.1016/j.jmr.2019.02.007.

## References

[1] C.P. Jaroniec, B.A. Tounge, J. Herzfeld, R.G. Griffin, frequency selective heteronuclear dipolar recoupling in rotating solids: accurate $^{13}C$–$^{15}N$ distance measurements in uniformly $^{13}C$,$^{15}N$-labeled peptides, J. Am. Chem. Soc. 123 (2001) 3507–3519.
[2] C.M. Rienstra, M. Hohwy, L.J. Mueller, C.P. Jaroniec, B. Reif, R.G. Griffin, Determination of multiple torsion-angle constraints in U–$^{13}C$,$^{15}N$-labeled peptides: 3D $^{1}H$–$^{15}N$–$^{13}C$–$^{1}H$ dipolar chemical shift NMR spectroscopy in rotating solids, J. Am. Chem. Soc. 124 (2002) 11908–11922.
[3] W.-W. Cai, R.D. Piner, F.J. Stadermann, S. Park, M.A. Shaibat, Y. Ishii, D.-X. Yang, A. Velamakanni, S.J. An, M. Stoller, J. An, D.-M. Chen, R.S. Ruoff, Synthesis and solid-state NMR structural characterization of $^{13}C$-labeled graphite oxide, Science 321 (2008) 1815–1817.
[4] X.-W. Fang, K. Schmidt-Rohr, Fate of the amino acid in glucose–glycine melanoidins investigated by solid-state nuclear magnetic resonance (NMR), J. Agric. Food Chem. 57 (2009) 10701–10711.
[5] N. Baccile, G. Laurent, F. Babonneau, F. Fayon, M.-M. Titirici, M. Antonietti, Structural characterization of hydrothermal carbon spheres by advanced solid-state MAS $^{13}C$ NMR investigations, J. Phys. Chem. C 113 (2009) 9644–9654.
[6] J.M. Anderson, R.L. Johnson, K. Schmidt-Rohr, B.H. Shanks, Solid state NMR study of chemical structure and hydrothermal deactivation of moderate-temperature carbon materials with acidic $SO_3H$ sites, Carbon 74 (2014) 333–345.
[7] R.L. Johnson, J.M. Anderson, B.H. Shanks, K. Schmidt-Rohr, Simple one-step synthesis of aromatic-rich materials with high concentrations of hydrothermally stable catalytic sites, validated by NMR, Chem. Mater. 26 (2014) 5523–5532.
[8] IsoLife – Stable Isotope Labelled Plant Products for the Life Sciences, in.
[9] H.N. Pham, A.E. Anderson, R.L. Johnson, K. Schmidt-Rohr, A.K. Datye, Improved hydrothermal stability of mesoporous oxides for reactions in the aqueous phase, Angew. Chem., Int. Ed. 51 (2012) 13163–13167.
[10] X.-K. Zhang, H.-L. Wang, L.-Z. He, K.-P. Lu, A. Sarmah, J.-U. Li, N.S. Bolan, J.-C. Pei, H.-G. Huang, Using biochar for remediation of soils contaminated with heavy metals and organic pollutants, Environ. Sci. Pollut. Res. 20 (2013) 8472–8483.
[11] M. Ahmad, A.U. Rajapaksha, J.E. Lim, M. Zhang, N. Bolan, D. Mohan, M. Vithanage, S.S. Lee, Y.S. Ok, Biochar as a sorbent for contaminant management in soil and water: a review, Chemosphere 99 (2014) 19–33.
[12] Y.S. Hu, R. Demir-Cakan, M.M. Titirici, J.O. Müller, R. Schlögl, M. Antonietti, J. Maier, Superior storage performance of a Si@$SiO_x$/C nanocomposite as anode material for lithium-ion batteries, Angew. Chem., Int. Ed. 47 (2008) 1645–1649.
[13] J.-J. Wang, X.-L. Sun, Understanding and recent development of carbon coating on $LiFePO_4$ cathode materials for lithium-ion batteries, Energy Environ. Sci. 5 (2012) 5163–5185.
[14] E. Raymundo-Piñero, M. Cadek, F. Béguin, Tuning carbon materials for supercapacitors by direct pyrolysis of seaweeds, Adv. Funct. Mater. 19 (2009) 1032–1039.
[15] L.-F. Chen, Z.-H. Huang, H.-W. Liang, W.-T. Yao, Z.-Y. Yu, S.-H. Yu, Flexible all-solid-state high-power supercapacitor fabricated with nitrogen-doped carbon nanofiber electrode material derived from bacterial cellulose, Energy Environ. Sci. 6 (2013) 3331–3338.
[16] H.-L. Wang, Z.-W. Xu, A. Kohandehghan, Z. Li, K. Cui, X.-H. Tan, T.J. Stephenson, C.K. King'ondu, C.M.B. Holt, B.C. Olsen, J.K. Tak, D. Harfield, A.O. Anyia, D. Mitlin, Interconnected carbon nanosheets derived from hemp for ultrafast supercapacitors with high energy, ACS Nano 7 (2013) 5131–5141.
[17] Y. Sun, P.A. Webley, Preparation of activated carbons from corncob with large specific surface area by a variety of chemical activators and their application in gas storage, Chem. Eng. J. 162 (2010) 883–892.
[18] A. Chuntanapum, Y. Matsumura, Formation of tarry material from 5-HMF in subcritical and supercritical water, Ind. Eng. Chem. Res. 48 (2009) 9837–9846.
[19] M. Sevilla, A.B. Fuertes, Chemical and structural properties of carbonaceous products obtained by hydrothermal carbonization of saccharides, Chem. Eur. J. 15 (2009) 4195–4203.
[20] K.G. Latham, M.I. Simone, W.M. Dose, J.A. Allen, S.W. Donne, Synchrotron based NEXAFS study on nitrogen doped hydrothermal carbon: insights into surface functionalities and formation mechanisms, Carbon 114 (2017) 566–578.
[21] C.M. Rienstra, M.E. Hatcher, L.J. Mueller, Sun, S.W. Fesik, R.G. Griffin, Efficient multispin homonuclear double-quantum recoupling for magic-angle spinning NMR: $^{13}C$–$^{13}C$ correlation spectroscopy of U-$^{13}C$-erythromycin A, J. Am. Chem. Soc. 120 (1998) 10602–10612.
[22] T.I. Igumenova, A.E. McDermott, K.W. Zilm, R.W. Martin, E.K. Paulson, A.J. Wand, Assignments of carbon NMR resonances for microcrystalline ubiquitin, J. Am. Chem. Soc. 126 (2004) 6720–6727.
[23] K. Schmidt-Rohr, K.J. Fritzsching, S.-Y. Liao, M. Hong, Spectral editing of two-dimensional magic-angle-spinning solid-state NMR spectra for protein resonance assignment and structure determination, J. Biomol. NMR 54 (2012) 343–353.
[24] R.L. Johnson, J.M. Anderson, B.H. Shanks, X.-W. Fang, M. Hong, K. Schmidt-Rohr, Spectrally edited 2D $^{13}C$–$^{13}C$ NMR spectra without diagonal ridge for characterizing $^{13}C$-enriched low-temperature carbon materials, J. Magn. Reson. 234 (2013) 112–124.
[25] J.K. Williams, K. Schmidt-Rohr, M. Hong, Aromatic spectral editing techniques for magic-angle-spinning solid-state NMR spectroscopy of uniformly $^{13}C$-labeled proteins, Solid State Nucl. Magn. Reson. 72 (2015) 118–126.
[26] Q. Chen, S.S. Hou, K. Schmidt-Rohr, A simple scheme for probehead background suppression in one-pulse $^{1}H$ NMR, Solid State Nucl. Magn. Reson. 26 (2004) 11–15.
[27] P. Duan, K. Schmidt-Rohr, Composite-pulse and partially dipolar dephased multiCP for improved quantitative solid-state $^{13}C$ NMR, J. Magn. Reson. 285 (2017) 68–78.
[28] T. Gullion, J. Schaefer, Rotational-echo double-resonance NMR, J. Magn. Reson. 81 (1989) 196–200.
[29] X.-L. Yao, K. Schmidt-Rohr, M. Hong, Medium- and long-distance $^{1}H$–$^{13}C$ heteronuclear correlation NMR in solids, J. Magn. Reson. 149 (2001) 139–143.
[30] P. Tekely, J. Brondeau, K. Elbayed, A. Retournard, D. Canet, A simple pulse train, using 90° hard pulses, for selective excitation in high-resolution solid-state NMR, J. Magn. Reson. 80 (1988) 509–516.
[31] E.R. deAzevedo, W.-G. Hu, T.J. Bonagamba, K. Schmidt-Rohr, Principles of centerband-only detection of exchange in solid-state nuclear magnetic resonance, and extension to four-time centerband-only detection of exchange, J. Chem. Phys. 112 (2000) 8988–9001.